



**HAL**  
open science

## Estimation of time delay and interface roughness by GPR using modified MUSIC

Meng Sun, Cédric Le Bastard, Nicolas Pinel, Yide Wang, Jianzhong Li,  
Jingjing Pan, Zhiwen Yu

► **To cite this version:**

Meng Sun, Cédric Le Bastard, Nicolas Pinel, Yide Wang, Jianzhong Li, et al.. Estimation of time delay and interface roughness by GPR using modified MUSIC. *Signal Processing*, 2017, 132, pp.272 - 283. 10.1016/j.sigpro.2016.05.029 . hal-01400510

**HAL Id: hal-01400510**

**<https://univ-rennes.hal.science/hal-01400510>**

Submitted on 22 Nov 2016

**HAL** is a multi-disciplinary open access archive for the deposit and dissemination of scientific research documents, whether they are published or not. The documents may come from teaching and research institutions in France or abroad, or from public or private research centers.

L'archive ouverte pluridisciplinaire **HAL**, est destinée au dépôt et à la diffusion de documents scientifiques de niveau recherche, publiés ou non, émanant des établissements d'enseignement et de recherche français ou étrangers, des laboratoires publics ou privés.

# Estimation of time delay and interface roughness by GPR using modified MUSIC

Meng Sun<sup>a</sup>, Cédric Le Bastard<sup>b,a</sup>, Nicolas Pinel<sup>c</sup>, Yide Wang<sup>a</sup>, Jianzhong Li<sup>a,d</sup>,  
Jingjing Pan<sup>a</sup>, Zhiwen Yu<sup>d</sup>

<sup>a</sup>*Institut d' Electronique et Télécommunications de Rennes (IETR), LUNAM Université  
Université de Nantes, UMR CNRS 6164, Rue Christian Pauc BP 50609, Nantes 44306, France  
Email:(jianzhong.li@etu.univ-nantes.fr)*

<sup>b</sup>*Cerema (Centre for expertise and engineering on risks, environment, mobility, urban and country  
planning), 23 avenue de l'Amiral Chauvin, BP 69, 49136 Les Ponts de Cé, France.*

<sup>c</sup>*Alyotech, 2 rue Antoine Becquerel, 35700 Rennes, France.*

<sup>d</sup>*South China University of Technology, Guangzhou 510641, Peoples Republic of China*

---

## Abstract

In civil engineering, roadway structure evaluation is an important application which can be carried out by ground penetrating radar. In this paper, firstly a signal model taking into account the influence of interfaces roughness (surface and interlayer) is proposed. In order to estimate the time delay and interface roughness, we propose a method composed of 2 steps: 1) a modified MUSIC algorithm is proposed for time delay estimation; 2) the interface roughness is estimated by using Maximum Likelihood method (MLE) with the estimated time delays. The proposed algorithms are tested on data obtained by a method of moments (MoM). Numerical examples are provided to demonstrate the performance of the proposed algorithm.

*Keywords:* Ground Penetrating Radar (GPR), Time-Delay Estimation (TDE), Roughness, modified MUSIC, Method of Moments (MoM), Maximum Likelihood method (MLE).

---

## 1. Introduction

Ground penetrating radar (GPR) is widely used as a non destructive testing technique for road pavement survey [1, 2, 3, 4, 5, 6], particularly for the measurement of different layer thicknesses. In road pavement survey, the road layers are assumed to be horizontally stratified [7]. Useful information about the vertical structure of the roadway can then be extracted from radar profiles by means of echo detection and amplitude estimation [8, 9, 10, 11]. Echo detection provides the time-delay estimation (TDE) associated with each interface, while amplitude estimation allows retrieving the wave speed within each layer. In this paper, we focus on the practical case when the backscattered echoes are overlapped [12, 13], which means that the thickness is smaller than the wavelength in the medium. In this case, high resolution and superresolution methods [14, 15, 16, 17] (or subspace methods) can be used to estimate the time delays of echoes and then to measure the small pavement thicknesses (with estimated permittivity). However, these methods assume that the interfaces of the layers are flat. For decimetre-scale GPR wavelengths (in the air), this assumption can be held, but for an ultra-wide band radar, this is no longer suitable. The influence of interface roughness and heterogeneous of medium must then be analysed [13, 18, 19]. In this paper, only the interface roughness is discussed. For large frequency bands, the case of a heterogeneous medium case can be considered as a homogeneous medium with an equivalent permittivity. The heterogeneity medium will be studied in future work. The interface roughness is characterized by a particular frequency signature of echoes amplitudes, which is decreasing with frequency. In this paper, we propose to firstly estimate the time delays and then the interface roughness with an ultra-wideband GPR. In the following, the media are

25 assumed to be lossless [20, 21]. Roughness parameter is important for road safety, like pavement skid resistance analysis, and for analysing the inside of the pavement, especially to detect the cracks or debondings by highlighting the disaggregation of interface materials.

In [19, 20], this kind of work has already been carried out, but the frequency  
30 behaviour coming from the roughness has been simply approximated by an exponential function (using a curve fitting method). In this situation, the high resolution methods can easily be applied for parameters estimation (time delays and roughness). Nevertheless, it is suitable only for narrow band (less than 2 GHz). With the widening of the frequency band, the curve fitting error will increase rapidly, which  
35 may bring errors to the interface roughness estimation. In order to reduce the errors coming from the curve fitting, we propose a modified MUSIC algorithm which can take into account several possible frequency behaviours, more adaptable for ultra-wideband GPR. Like in [19, 20], we also focus on the estimation of time delays and interface roughness. Unlike the methods in [19, 20], the proposed method allows es-  
40 timating the time delays without knowing the frequency behaviour from roughness. Then, the roughness parameter is estimated by MLE [22] with the estimated time delays from the modified MUSIC algorithm. This step uses a model of which the roughness frequency behaviour is approximated as a Gaussian function. The performance of the proposed algorithm is tested on data simulated from PILE method  
45 [13, 23, 24, 25], which is based on the method of moments.

This paper is organised as follows. Section 2 gives the simulation results of the scattering of EM waves from random rough interfaces, and studies the frequency behaviour of the backscattered echoes. In section 3, the radar data model and

preprocessing methods are presented. In section 4, a modified MUSIC algorithm  
 50 is proposed to estimate the time delays without knowing the frequency behaviour.  
 Moreover, the roughness parameters are estimated by MLE [22]. Simulation results  
 and a discussion on the performance of the proposed algorithm are given in section  
 5. Finally, conclusions and perspectives are drawn.

## 2. Rough pavement scattering model

55 In order to give some ideas about the scattering from a rough pavement, a realistic  
 simulation of a typical thin asphalt road structure (pavement layer) is considered.  
 The rigorous electromagnetic method PILE (propagation inside layer expansion)  
 [23, 25] based on the MoM, provides simulation data that allows showing the influence  
 of the interface roughness on the backscattered echoes of stratified media. The  
 60 simulation parameters are chosen to match the air-coupled radar configuration at  
 vertical incidence that is used for pavement survey at traffic speed; the probing  
 scope is assumed to be limited to the first two layers of the pavement structure. The  
 considered pavement structure is an Ultra-Thin Asphalt Surfacing (UTAS), which  
 is made of a layer medium  $\Omega_2$  with mean thickness  $\bar{H} = 20$  mm. For the rolling  
 65 band (or base band) corresponding to the medium  $\Omega_3$ , it has the same composition  
 as the medium  $\Omega_2$ , see Fig. 1. We assume that  $\Omega_2$  and  $\Omega_3$  are homogeneous media  
 for a normal incidence angle ( $\theta_i=0$  in Fig. 1) and the frequency band under study  
 is  $[0.5, 10.5]$  GHz. For the considered media, their relative permittivity  $\varepsilon_r$  typically  
 ranges between 4 and 8. Moreover, in this paper, the media are assumed to be lossless.  
 70 For the simulations, we take  $\varepsilon_{r2} = 4.5$  and  $\varepsilon_{r3} = 7$ . The two rough interfaces  $\Sigma_A$   
 and  $\Sigma_B$  are assumed to have a Gaussian height probability density function and an

exponential height autocorrelation function [26, 27]. For  $\Sigma_A$ , the RMS height  $\sigma_{hA}$  is about 0.6 – 1 mm, and the correlation length  $L_{cA}$  is about 5 – 10 mm [26, 27]. For  $\Sigma_B$ , the RMS height  $\sigma_{hB}$  and the correlation length  $L_{cB}$  are greater than those of  $\Sigma_A$ . It is assumed that the antenna radiates a vertically polarized plane wave in far field of probed pavement (in practice, the antenna is about 400 mm above the rough surface). The typical width of a probed surface antenna footprint is about 300 – 500 mm. In the simulations, we consider surfaces of length  $L = 2400$  mm, illuminated by a Thorsos beam (the Thorsos beam is a tapered plane wave, whose tapering has a Gaussian shape; the tapering is used to reduce the incident field to near zero at the edges of the surface realisations and thereby to reduce edge effects to negligible levels) of attenuation parameter  $g = L/8$ . The two rough interfaces are sampled with a sampling step  $\Delta x = Re(\lambda_2)/8$ , where  $\lambda_2$  is the wavelength inside  $\Omega_2$  with  $\lambda_2 = \lambda_0/\sqrt{\varepsilon_{r2}}$  ( $\lambda_0$  is the wavelength in vacuum) and  $Re(\dots)$  is the real part. We take an incident wave with normal incidence ( $\theta_i = 0$ ), and then calculate the first two scattered echoes  $s_1$  and  $s_2$  from the scattered field.

In order to investigate the influence of interface roughness on the backscattered echoes, a rough pavement is tested, with roughness parameters  $\sigma_{hA} = 1.0$  mm,  $L_{cA} = 6.4$  mm,  $\sigma_{hB} = 2.0$  mm,  $L_{cB} = 15$  mm. According to the selected parameters, PILE method provides the first two backscattered echoes  $s_1$  and  $s_2$  at each frequency over the frequency band  $f \in [0.5, 10.5]$  GHz, with sampling step  $\Delta f = 0.1$  GHz. Simulated data were obtained by a Monte Carlo process with 100 independent realizations. Two models are presented: an exponential shape and a Gaussian shape. For doing so, a curve fitting is made by using least squares method to estimate the parameters of the model. In [19, 20], the exponential shape  $|s(f)| = s_k \times \exp(-\bar{b}f)$

with roughness parameter  $\bar{b}$  of the scattered echo amplitude is studied. In this paper, we introduce a Gaussian shape  $|s(f)| = s_k \times \exp(-bf^2)$  with a different roughness parameter  $b$ ; where  $s_k$  is the amplitude of the considered backscattered echo in the flat pavement.

100 Curve fittings are made with radar data from PILE in 3 narrow bands ( $f \in [0.5, 1.5]$  GHz,  $f \in [0.5, 2.5]$  GHz,  $f \in [0.5, 3.5]$  GHz) and 3 large frequency bands ( $f \in [0.5, 6.5]$  GHz,  $f \in [0.5, 8.5]$  GHz,  $f \in [0.5, 10.5]$  GHz). Figs. 2 and 3 give the frequency behaviour of the backscatter echoes. We can notice that the amplitudes of the backscattered echoes are decreasing when the frequency increases, especially for  
 105 the second echo. Thus, the influence of the interface roughness cannot be neglected any more, the frequency behaviour of the echoes should be considered in radar data processing. In addition, Figs. 2 and 3 also show the curve fitting results of the Gaussian and exponential functions. It can be noticed that, the Gaussian fitting is generally in good agreement with radar data in the whole frequency band, but  
 110 for the exponential fitting, significant deviations can be found, particularly for large frequency bands. We assess the performance of the curve fitting by Root Means Square Errors (RMSE), as shown in Table. 1. The results are in agreement with the above figures, the Gaussian fitting is more precise than the exponential fitting.

### 3. Signal model

In the previous section, the frequency behaviour of interface roughness has been studied by using PILE method. In this paper, we focus on the first two or three top layers of roadway, the whole thickness (of the roadway) is about 6 to 13 cm. Indeed, in our study, we focus on pavements which are composed of an ultra-thin

asphalt surface (1 to 3 cm thickness) and a base course (5 to 10 cm thickness). For pavement materials, according to the data provided in [28], the conductivity usually ranges within the interval  $[10^{-3}; 10^{-2}]$  S/m. Thus, the media considered in this paper are assumed to be low-loss media. Moreover, the pavement permittivity remains constant within the GPR bandwidth and generally ranges between 4 and 8. Thus, the considered media are low-loss and non-dispersive media. In addition, the dispersivity of the medium can be neglected [29], if the surface medium is slightly lossy. For flat pavements, the backscattered echoes can be simply considered as time-shifted and attenuated copies of the transmitted signal [9, 12, 21, 30]. For a rough pavement, a new signal model is presented with roughness for non-dispersive media and without considering the conductivity as follows:

$$r(f_i) = \sum_{k=1}^K e(f_i) s_k w_k(f_i) \exp(-j2\pi f_i t_k) + n(f_i) \quad (1)$$

115 where

- $K$  is the number of interfaces;
- $e(f_i)$  is the radar pulse at frequency  $f_i$ ;
- $s_k$  represents the reflection coefficient of the  $k$ th scattered echo with flat interfaces, which is independent of  $f_i$ ;
- 120 •  $n(f_i)$  is an additive white Gaussian noise, with zero mean and variance  $\sigma^2$ ;
- $w_k(f_i)$  represents the frequency behaviour of the  $k$ th scattered echo at frequency  $f_i = f_1 + (i - 1)\Delta f$  and  $i = 1, 2 \dots N$ ,  $N$  being the number of used frequencies;

$f_1$  is the lowest frequency of the studied frequency band and  $\Delta f$  is the frequency step.

125 Eq. (1) can be written in the following vector form:

$$\mathbf{r} = \mathbf{\Lambda} \mathbf{A} \mathbf{s} + \mathbf{n} \quad (2)$$

with the following notation definitions:

- $\mathbf{r} = [r(f_1) \ r(f_2) \ \cdots \ r(f_N)]^T$  is the  $(N \times 1)$  received signal vector, called observation vector, which may represent either the Fourier transform of the GPR signal or the measurements from a step frequency radar; the superscript  $T$  denotes the transpose operator;
- $\mathbf{\Lambda} = \text{diag}(e(f_1), e(f_2), \dots, e(f_N))$  is a  $(N \times N)$  diagonal matrix, whose diagonal elements are the Fourier transform  $e(f)$  of the radar pulse  $e(t)$ ;
- $\mathbf{A} = [\mathbf{a}(t_1) \ \mathbf{a}(t_2) \ \dots \ \mathbf{a}(t_K)]$  is called the  $(N \times K)$  mode matrix;
- $\mathbf{a}(t_k) = [\exp(-2j\pi f_1 t_k) w_k(f_1) \ \exp(-2j\pi f_2 t_k) w_k(f_2) \ \dots \ \exp(-2j\pi f_N t_k) w_k(f_N)]^T$  is the mode vector;
- $\mathbf{s} = [s_1 \ s_2 \ \cdots \ s_K]^T$  is the  $(K \times 1)$  vector of echoes amplitudes in the case of flat interfaces;
- $\mathbf{n} = [n(f_1) \ n(f_2) \ \cdots \ n(f_N)]^T$  is the  $(N \times 1)$  noise vector, with variance matrix  $\sigma^2 \mathbf{I}$ ;

140 According to signal model (2) and assuming that the noise is independent of the echoes, the covariance matrix  $\mathbf{Y}$  can be written as:

$$\begin{aligned}\mathbf{Y} &= E(\mathbf{r}\mathbf{r}^H) = \mathbf{\Lambda}\mathbf{A}E(\mathbf{s}\mathbf{s}^H)\mathbf{A}^H\mathbf{\Lambda}^H + E(\mathbf{n}\mathbf{n}^H) \\ &= \mathbf{\Lambda}\mathbf{A}\mathbf{S}\mathbf{A}^H\mathbf{\Lambda}^H + \sigma^2\mathbf{I}\end{aligned}\quad (3)$$

where  $E(\cdot)$  denotes the ensemble average,  $\mathbf{S}$  is the  $K \times K$  dimensional covariance matrix of the source vector  $\mathbf{s}$  and  $\mathbf{I}$  is an identity matrix. In the following, the data are divided by the pulse, thus the new observation vector  $\mathbf{r}'$  can be written as  $\mathbf{r}' = \mathbf{\Lambda}^{-1}\mathbf{r} = \mathbf{A}\mathbf{s} + \mathbf{\Lambda}^{-1}\mathbf{n} = \mathbf{A}\mathbf{s} + \mathbf{b}$ , where  $\mathbf{b}$  is the new noise vector after division. Thus, the new covariance matrix  $\mathbf{R}_0$  can be written as:

$$\mathbf{R}_0 = E(\mathbf{r}'\mathbf{r}'^H) = \mathbf{\Lambda}^{-1}\mathbf{Y}\mathbf{\Lambda}^{-H} = \mathbf{A}\mathbf{S}\mathbf{A}^H + \sigma^2\mathbf{\Sigma}\quad (4)$$

with

$$\mathbf{\Sigma} = \mathbf{\Lambda}^{-1}\mathbf{\Lambda}^{-H} = \text{diag}\left(\frac{1}{|e(f_1)|^2}, \frac{1}{|e(f_2)|^2}, \dots, \frac{1}{|e(f_N)|^2}\right)\quad (5)$$

In practice, the correlation between echoes degrades the subspace algorithm's performance. In this situation, preprocessing methods like spatial smoothing technique are used to obtain a new covariance matrix of restored rank. This kind of techniques only works on uniform linear frequency behaviours [31]. As the frequency behaviour of backscattered echoes  $w(f)$  can have an arbitrary frequency behaviour, methods like spatial smoothing technique cannot be used directly. In order to solve this problem, we propose to interpolate the frequency behaviour of backscattered

echoes into a uniform linear. Then, the spatial smoothing technique can be applied. This kind of algorithms is called interpolated spatial smoothing technique [32, 33]. By using interpolation, a new covariance matrix can be written as follows:

$$\bar{\mathbf{R}} = \mathbf{B}\mathbf{A}\mathbf{S}\mathbf{A}^H\mathbf{B}^H + \sigma^2\mathbf{B}\Sigma\mathbf{B}^H \quad (6)$$

where  $\mathbf{B}$  is a transformation matrix of interpolation (the details of the interpolation are provided in appendix A). In the following section, a modified MUSIC algorithm is proposed and applied for time delay estimation. This method assumes that the noise is a Gaussian white noise. To ensure this condition, like in [20], the noise covariance matrix should be removed. As the radar pulse (measured by the echo backscattered from a metallic plane) and the transformation matrix  $\mathbf{B}$  are known, and the noise variance  $\sigma^2$  is estimated by the propagator method [34], the new noise free covariance matrix  $\mathbf{R}$  can be written as follows:

$$\mathbf{R} = \mathbf{B}\mathbf{A}\mathbf{S}\mathbf{A}^H\mathbf{B}^H + 0 \times \mathbf{I} \approx \bar{\mathbf{R}} - \hat{\sigma}^2\mathbf{B}\Sigma\mathbf{B}^H \quad (7)$$

where  $\hat{\sigma}^2$  is the estimated noise variance. Then, the spatial smoothing preprocessing technique can be applied [35]. The SSP technique estimates the modified covariance matrix  $\mathbf{R}_{SSP}$  as follows [35]:

$$\mathbf{R}_{SSP} = \frac{1}{M} \sum_{k=1}^M \mathbf{R}_k \quad (8)$$

where  $\mathbf{R}_k$  is the  $k^{th}$  sub-band of the covariance matrix  $\mathbf{R}$ ,  $N$  frequencies,  $M$  overlapping sub-bands of length  $L$  are considered.  $N$ ,  $M$  and  $L$  are related to one another

by:

$$N = L + M - 1$$

#### 4. Time delay and interface roughness estimation

When the interface roughness is taken into account, high resolution algorithms  
 145 like MUSIC or ESPRIT cannot be used directly in theory, due to the unknown  
 frequency behaviour  $w_k(f_i)$  of the echoes. Therefore, we propose a modified MUSIC  
 algorithm to estimate the time delays, and then MLE is used to estimate the interface  
 roughness.

##### 4.1. Modified MUSIC algorithm

In this section, a modified MUSIC algorithm is proposed, which allows estimating  
 only the time delays. The mode vector  $\mathbf{a}$  can be written as follows:

$$\begin{aligned} \mathbf{a}(t) &= [\exp(-2j\pi f_1 t)\bar{w}(f_1) \quad \exp(-2j\pi f_2 t)\bar{w}(f_2) \\ &\quad \dots \quad \exp(-2j\pi f_L t)\bar{w}(f_L)]^T \\ &= \text{diag}\{\exp(-2j\pi f_1 t), \exp(-2j\pi f_2 t) \dots, \exp(-2j\pi f_L t)\} \\ &\quad [\bar{w}(f_1)\bar{w}(f_2) \quad \dots \quad \bar{w}(f_L)]^T \\ &= \widehat{\mathbf{A}}\mathbf{k} \end{aligned}$$

where  $\widehat{\mathbf{A}} = \text{diag}\{\exp(-2j\pi f_1 t), \exp(-2j\pi f_2 t), \dots, \exp(-2j\pi f_L t)\}$  and  $\mathbf{k} = [\bar{w}(f_1)\bar{w}(f_2) \quad \dots \quad \bar{w}(f_L)]^T$   
 with  $\bar{w}(f)$  the frequency behaviour of the backscattered echoes after interpolation.  
 $\mathbf{k}$  is a real vector.

The pseudo-spectrum of MUSIC can be written as:

$$P(t) = [\min_k \{ \frac{\mathbf{k}^H \widehat{\mathbf{A}}^H \mathbf{U}_N \mathbf{U}_N^H \widehat{\mathbf{A}} \mathbf{k}}{\mathbf{k}^H \widehat{\mathbf{A}}^H \widehat{\mathbf{A}} \mathbf{k}} \}]^{-1} \quad (9)$$

150 where  $U_N$  is the  $L \times (L - K)$  noise matrix whose columns are the  $L - K$  noise eigenvectors. Referring to [36],  $P(t)$  is equal to the minimum generalized eigenvalue  $\lambda_{min}$  of  $\widehat{\mathbf{A}}^H \mathbf{U}_N \mathbf{U}_N^H \widehat{\mathbf{A}}$  and  $\widehat{\mathbf{A}}^H \widehat{\mathbf{A}}$ , satisfying (with  $\mathbf{k}_{min}$  the corresponding generalized eigenvector):

$$\widehat{\mathbf{A}}^H \mathbf{U}_N \mathbf{U}_N^H \widehat{\mathbf{A}} \mathbf{k}_{min} = \lambda_{min} \widehat{\mathbf{A}}^H \widehat{\mathbf{A}} \mathbf{k}_{min} = \lambda_{min} \mathbf{k}_{min} \quad (10)$$

The pseudo-spectrum of MUSIC can also be written as the reciprocal of the minimum eigenvalue of  $\text{real}\{\widehat{\mathbf{A}}^H \mathbf{U}_N \mathbf{U}_N^H \widehat{\mathbf{A}}\}$  [36, 37]:

$$P(t) = \frac{1}{\lambda_{min}(t)} \quad (11)$$

By using (11), we need only to search the spectrum in the time domain without knowing the influence of the frequency behaviour. Nevertheless, it has a false peak in the middle of two true values. For example, when two echoes are considered, we assume that  $t_1$  and  $t_2$  ( $t_2 > t_1$ ) are the time delays of the echoes, then we can prove that  $t_3 = \frac{t_2 - t_1}{2}$  is also a solution of  $\lambda_{min}(t) = 0$  (the proof is given in appendix B). In [37], based on the characteristics of  $\lambda_{min}(t)$  corresponding to the false time delay and the true time delays, they propose a new pseudo-spectrum of MUSIC to cancel

the false time delay, which can be expressed as follows:

$$P(t) = 10 \log_{10} \left\{ \frac{\lambda_1(t)}{\lambda_2(t)} \right\} \quad (12)$$

where  $\lambda_k(t)$  is the  $k$ th eigenvalue of  $\text{real}\{\widehat{\mathbf{A}}^H \mathbf{U}_N \mathbf{U}_N^H \widehat{\mathbf{A}}\}$ , and  $\lambda_L(t) \geq \lambda_{L-1}(t) \geq \dots \geq \lambda_1(t)$ . Still, the above method only works for the case of two echoes. Indeed, for the case where the number of echoes is superior to 2, eq. (12) does not work. For example, when a true time delay has the same value as a false one, this true time delay will also be cancelled. From appendix B, we show that the number of zero eigenvalues of  $\text{real}\{\widehat{\mathbf{A}}^H \mathbf{U}_N \mathbf{U}_N^H \widehat{\mathbf{A}}\}$  corresponding to the true time delay is odd, and to the false time delay, this number is even. Based on the above characteristics, we propose a generalized pseudo-spectrum for modified MUSIC as follows:

$$P(t) = \begin{cases} \frac{\lambda_2(t) \lambda_4(t) \cdots \lambda_{L-1}(t)}{\lambda_1(t) \lambda_3(t) \cdots \lambda_{L-2}(t)} & L = 2n + 1 \\ \frac{\lambda_2(t) \lambda_4(t) \cdots \lambda_L(t)}{\lambda_1(t) \lambda_3(t) \cdots \lambda_{L-1}(t)} & L = 2n \end{cases} \quad (13)$$

where  $n = 0, 1, 2, \dots$  and  $L$  can be an odd or even number. The pseudo-spectrums of  
 155 MUSIC in (11), (12) and (13) are shown in Fig. 4. In the simulation, 3 time delays  
 (1 ns, 1.3 ns and 1.6 ns) are considered, the second time delay is in the middle of  
 the other two time delays. In order to make a better comparison between the three  
 pseudo-spectrums, an amplitude normalization is made in Fig. 4. Modified MUSIC  
 in (11) obtains two false peaks at 1.15 ns and 1.45 ns. By using (12), the two false  
 160 peaks are removed, but also the second time delay. Only the proposed method (13)  
 can successfully remove the false time delays and keep the true time delays. Thus,

Eq. (13) is used in the following of the paper.

#### 4.2. MLE for roughness parameter estimation

For the frequency behaviour of backscattered echoes, it has been found in the previous section that the frequency behaviour  $w(f)$  can be approximated by a Gaussian function for ultra wide band radar. It enables a parametrization of the frequency variations for data modelling. We assume that the frequency behaviour can be expressed as  $w_k(f_i) = \exp(-b_k f_i^2)$ , where  $b_k$  is the roughness parameter of the  $k$ th interface. For flat interfaces,  $b_k = 0$ . This parameter can be calculated by MLE [22] with estimated time delays, the details of the calculation are given in appendix C. We should notice that the roughness parameters are very sensitive to the bias of the estimated time delay, especially when the roughness parameters are very small, as shown in Figure. 5 (only the first layer is considered). Note that when the value of  $T_1$  is not the true value, the relative-root-mean-square error (RRMSE) on roughness parameter  $b_1$  increases drastically.

## 5. Simulations and discussion

In the simulations, the performance of the modified MUSIC and MLE is tested on the data provided by PILE method. The simulated data represent the radar backscattered signal at nadir from a rough pavement made of two rough interfaces separating homogeneous media. The studied pavement structure is made of a layer of ultra thin asphalt surfacing with a relative permittivity equal to 4.5 overlying a base band with a relative permittivity equal to 7. We consider two scattered echoes corresponding to the time delays 1 ns and 1.3 ns, which corresponds to thickness

of the first layer of approximately 20 mm and the second layer is infinite. In the  
 185 simulations, four pavements are studied (the rough interfaces are assumed to have a  
 Gaussian height probability density function and an exponential height autocorrela-  
 tion function) [26, 27] with different root mean square heights  $\sigma_h$ , correlation lengths  
 $L_h$  and conductivities of the layers  $\delta$ :

- Case 1.  $\sigma_{hA} = 1.0$  mm,  $L_{cA} = 6.4$  mm,  $\sigma_{hB} = 2.0$  mm,  $L_{cB} = 15$  mm, lossless  
 190 media.
- Case 2.  $\sigma_{hA} = 1.0$  mm,  $L_{cA} = 6.4$  mm,  $\sigma_{hB} = 2.5$  mm,  $L_{cB} = 15$  mm, lossless  
 media.
- Case 3.  $\sigma_{hA} = 1.5$  mm,  $L_{cA} = 6.4$  mm,  $\sigma_{hB} = 3.0$  mm,  $L_{cB} = 15$  mm, lossless  
 media.
- Case 4.  $\sigma_{hA} = 1.0$  mm,  $L_{cA} = 6.4$  mm,  $\sigma_{hB} = 2.0$  mm,  $L_{cB} = 15$  mm, low-loss  
 195 media ( $\delta_A = 5 \times 10^{-3}$  S/m,  $\delta_B = 10^{-2}$  S/m).

When the frequency band is 0.5 – 3.5 GHz, with 0.05 GHz frequency step (61 fre-  
 quency samples), the echoes are slightly overlapped. When the frequency band is  
 0.5 – 6.5 GHz, with 0.1 GHz frequency step (61 frequency samples), the echoes are  
 200 non-overlapped. The covariance matrix is estimated from 1000 independent snap-  
 shots. The interpolated SSP technique is used to reduce the cross-correlation between  
 the echoes and the number of sub-bands ( $M$ ) is equal to 20. The signal-to-noise ra-  
 tio (SNR) is defined as the ratio between the powers of the second echo and noise  
 variance. In the first simulation, a fixed SNR=20 dB is used for three different rough  
 205 pavements.

Figs. 6-10 show the pseudo-spectrums of modified MUSIC. Two peaks corresponding to the time delays of the first two scattered echoes are well estimated. Simulation results demonstrate that the proposed algorithm can handle cases where both echoes are either overlapped or non-overlapped and for either lossless or low-loss media. The roughness parameters could also be estimated by using the MLE with the estimated time delays (see Figs. 11-15). Table. 2 gives the results of estimated time delays ( $\hat{t}_k$ ) and estimated roughness parameters ( $\hat{b}_k$ ). We compare the estimated frequency behaviours with the data from PILE in Figs. 11-15. From the frequency behaviour of the four different cases, it is shown that the expressions of the echoes are in agreement with the data from PILE for various roughness parameters with either lossless media or low-loss media.

Then, in the second simulation, we evaluate the performance of modified MUSIC, which is assessed with a Monte-Carlo process of 500 independent runs of the algorithm with independent noise snapshots and from the RRMSE of the evaluated parameter as follows:

$$RRMSE(z) = \frac{\sqrt{\frac{1}{U} \sum_{j=1}^U (\hat{z}_j - z)^2}}{z}, \quad (14)$$

where  $\hat{z}_j$  denotes the estimated parameter for the  $j$ th run of the algorithm, and  $z$  the true value. In the simulation, the parameter  $z$  can represent either the first ( $t_1$ ) or the second ( $t_2$ ) time delay. Only case 1 is considered. In the time delay estimation, as expected, it can be seen that the RRMSE is continuously decreasing when the SNR increases. Fig. 16 shows that the proposed method gives relatively good performances in time delay estimation.

In the third simulation, the performance of the proposed method is tested on a pavement which is composed of 3 rough interfaces (four layers). The simulation parameters of the pavement are chosen as follows: the permittivities of first three layers are  $\varepsilon_{r2} = 4.5$ ,  $\varepsilon_{r3} = 7$  and  $\varepsilon_{r4} = 9$ , respectively; we consider three backscattered echoes corresponding to the first three time delays 1 ns, 1.3 ns and 1.7 ns, which corresponds to a thickness of the second layer as approximately 20 mm, of the third layer as approximately 23 mm and of the fourth layer as infinite; the roughness parameters of three rough interfaces are chosen as follows:  $b_1 = 1.60 \times 10^{-3} \text{ GHz}^{-2}$ ,  $b_2 = 1.70 \times 10^{-2} \text{ GHz}^{-2}$  and  $b_3 = 3.00 \times 10^{-2} \text{ GHz}^{-2}$ , which are obtained from the signal model in Eq. 1. Figs. 17 and 18 present the pseudo-spectrum of the modified MUSIC and the frequency behaviour of the backscattered echoes for a rough pavement with 3 layers. It can be seen that the three peaks corresponding to the time delays of the first three scattered echoes are well estimated (estimated time delays are  $\hat{t}_1 = 0.999 \text{ ns}$ ,  $\hat{t}_2 = 1.302 \text{ ns}$  and  $\hat{t}_3 = 1.705 \text{ ns}$ ). Furthermore, the estimated frequency behaviours of backscattered echoes are in relatively good agreement with the data from signal model (estimated roughness parameters are  $\hat{b}_1 = 1.50 \times 10^{-3} \text{ GHz}^{-2}$ ,  $\hat{b}_2 = 1.83 \times 10^{-2} \text{ GHz}^{-2}$  and  $\hat{b}_3 = 2.93 \times 10^{-2} \text{ GHz}^{-2}$ ).

## 6. Conclusion

In this paper, we have studied time delays and interface roughness estimation with coherent backscattered echoes. After applying the interpolated spatial smoothing technique to decorrelate the received echoes, we propose a modified MUSIC algorithm, which is able to estimate the time delays without knowing the frequency behaviour from roughness. Then, the influence of the interface roughness is estimated

250 by MLE. These algorithms are applied to evaluate the pavement. The performance of the proposed algorithms is tested on data from MoM. The proposed algorithms show good performance for time delays and interface roughness estimation. In perspective, the proposed method will be extended to dispersive media (soils or hydraulic concretes).

## 255 Appendix A

The mode vector can be written as:

$$\begin{aligned} \mathbf{a}(t_k) &= [\exp(-2j\pi f_1 t_k) w_k(f_1) \exp(-2j\pi f_2 t_k) w_k(f_2) \dots \exp(-2j\pi f_N t_k) w_k(f_N)]^T \\ &= \text{diag}\{w_k(f_1), w_k(f_2) \dots w_k(f_N)\} [\exp(-2j\pi f_1 t_k), \exp(-2j\pi f_2 t_k) \dots \exp(-2j\pi f_N t_k)]^T \\ &= \mathbf{C}\bar{\mathbf{a}} \end{aligned}$$

The frequency behaviour  $w(f)$  depends on the RMS height  $\sigma_h$  and the correlation length  $L_h$ , thus matrix  $\mathbf{C}$  also changes with  $\sigma_h$  and  $L_h$ , it can be expressed as  $\mathbf{C}(\sigma_h, L_h)$ . We propose to interpolate  $w(f)$  into a uniform linear frequency behaviour. The procedure is as follows:

- 260 • Define a set of  $\sigma_h = \{\sigma_{h1}, \sigma_{h2} \dots \sigma_{hG}\}$  and a set of  $L_h = \{L_{h1}, L_{h2} \dots L_{hP}\}$ ;
- Compute the model vectors associated with the set  $\sigma_h$  and  $L_h$ , and arrange them into a matrix form as follows:

$$\mathbf{C}_r = [\mathbf{C}(\sigma_{h1}, L_{h1}) \mathbf{C}(\sigma_{h1}, L_{h2}) \dots \mathbf{C}(\sigma_{h1}, L_{hP}) \mathbf{C}(\sigma_{h2}, L_{h1}) \dots \mathbf{C}(\sigma_{hG}, L_{hP})];$$

- Decide where to place the "virtual elements" of the interpolation matrix.  $\mathbf{C}_v =$
- 265  $[\hat{\mathbf{C}}(\sigma_{h1}, L_{h1}) \hat{\mathbf{C}}(\sigma_{h1}, L_{h2}) \dots \hat{\mathbf{C}}(\sigma_{h1}, L_{hP}) \hat{\mathbf{C}}(\sigma_{h2}, L_{h1}) \dots \hat{\mathbf{C}}(\sigma_{hG}, L_{hP})], \hat{\mathbf{C}}(\sigma_h, L_h)$  has a uniform linear frequency behaviour.

- Find the transformation matrix  $\mathbf{B}$  by a least squares solution of  $\mathbf{B}\mathbf{C}_r = \mathbf{C}_v$ . The "best" interpolation matrix  $\mathbf{C}_v$  is the one which will minimize  $\|\mathbf{B}\mathbf{C}_r - \mathbf{C}_v\|^2$ .

## 270 Appendix B

In this appendix, we present why a false peak exists. Only the case of two echoes is presented, but the same calculation can be carried out when the number of echoes is superior to 2. We assume  $t_1$  and  $t_2$  are the time delays of two echoes ( $t_1 < t_2$ ) and define  $t_3 = (t_1 + t_2)/2$ ,  $\Delta t = (t_2 - t_1)/2$ ,  $\Phi(t) = \widehat{\mathbf{A}}^H(t)\mathbf{U}_N\mathbf{U}_N^H\widehat{\mathbf{A}}(t)$ .  
 275 By definition, the rank of  $\mathbf{U}_N\mathbf{U}_N^H$  is  $L - 2$ , it has always 2 zero eigenvalues with 2 eigenvectors,  $\mathbf{a}^H(t)\mathbf{U}_N\mathbf{U}_N^H\mathbf{a}(t)$  is real valued. Following the subspace principle, we have 2 equalities:

- $\mathbf{a}^H(t)\mathbf{U}_N\mathbf{U}_N^H\mathbf{a}(t) = \mathbf{k}^T\widehat{\mathbf{A}}^H(t)\mathbf{U}_N\mathbf{U}_N^H\widehat{\mathbf{A}}(t)\mathbf{k} = \mathbf{k}^T\Phi(t)\mathbf{k} = 0$ , for  $t = t_1$  or  $t_2$ .
- $\mathbf{k}^T\Phi(t)\mathbf{k} \neq 0$ , for  $t \neq t_1$  or  $t_2$ .

280 Then we can have the following 3 situations:

case 1:  $t = t_1$  and  $t_2$ . When  $t = t_1$  or  $t_2$ ,  $\mathbf{a}^H(t)\mathbf{U}_N\mathbf{U}_N^H\mathbf{a}(t) = \mathbf{k}^T\widehat{\mathbf{A}}^H(t)\mathbf{U}_N\mathbf{U}_N^H\widehat{\mathbf{A}}(t)\mathbf{k} = \mathbf{k}^T\Phi(t)\mathbf{k} = 0$ .  $\Phi(t)$  has 2 zero eigenvalues with 2 eigenvectors and  $\mathbf{k}$  is a real eigenvector. For  $t = t_1$ , we can see also:

$$\begin{aligned} & \mathbf{k}^T\widehat{\mathbf{A}}^H(t_2 - t_1)\widehat{\mathbf{A}}^H(t_1)\mathbf{U}_N\mathbf{U}_N^H\widehat{\mathbf{A}}(t_1)\widehat{\mathbf{A}}(t_2 - t_1)\mathbf{k} \\ & = \mathbf{k}_{10}^H\widehat{\mathbf{A}}^H(t_1)\mathbf{U}_N\mathbf{U}_N^H\widehat{\mathbf{A}}(t_1)\mathbf{k}_{10} = \mathbf{k}^T\widehat{\mathbf{A}}^H(t_2)\mathbf{U}_N\mathbf{U}_N^H\widehat{\mathbf{A}}(t_2)\mathbf{k} \end{aligned}$$

where  $\mathbf{k}_{10} = \widehat{\mathbf{A}}(t_2 - t_1)\mathbf{k}$  is another eigenvector. Similarly,  $\mathbf{k}_{20} = \widehat{\mathbf{A}}(t_1 - t_2)\mathbf{k}$  is the  
 285 second eigenvector for  $t = t_2$ .  $\mathbf{k}_{10}$  and  $\mathbf{k}_{20}$  are complex valued and not collinear with

$\mathbf{k}$ , any non-zero coefficients linear combination of  $\mathbf{k}$  and  $\mathbf{k}_{10}$  or  $\mathbf{k}$  and  $\mathbf{k}_{20}$  is complex valued. Therefore,  $\Phi(t)$  has only one real eigenvector ( $\mathbf{k}$ ) corresponding to one single zero eigenvalue, and  $real\{\mathbf{k}^T \Phi(t) \mathbf{k}\} = \mathbf{k}^T real\{\Phi(t)\} \mathbf{k} = 0$ , only one solution for  $t_1$  or  $t_2$ . Thus, the number of zero eigenvalue of  $real\{\Phi(t_1)\}$  and  $real\{\Phi(t_2)\}$  is 1.

290 case 2:  $t \neq t_1, t_2$  and  $t_3$ .  $\Phi(t)$  has 2 zero eigenvalues, we can find easily 2 non-linearly correlated eigenvectors  $\mathbf{k}_1$  and  $\mathbf{k}_2$  corresponding to the zero eigenvalues:

$$\begin{aligned}\mathbf{k}_1^H \Phi(t) \mathbf{k}_1 &= \mathbf{k}_1^H \widehat{\mathbf{A}}^H(t) \mathbf{U}_N \mathbf{U}_N^H \widehat{\mathbf{A}}(t) \mathbf{k}_1 = 0 \\ \mathbf{k}_2^H \Phi(t) \mathbf{k}_2 &= \mathbf{k}_2^H \widehat{\mathbf{A}}^H(t) \mathbf{U}_N \mathbf{U}_N^H \widehat{\mathbf{A}}(t) \mathbf{k}_2 = 0\end{aligned}$$

where  $\mathbf{k}_1 = \widehat{\mathbf{A}}(t_1 - t) \mathbf{k}$  and  $\mathbf{k}_2 = \widehat{\mathbf{A}}(t_2 - t) \mathbf{k}$ . Due to  $t \neq t_1, t_2$  and  $t_3$ ,  $\mathbf{k}_1$  and  $\mathbf{k}_2$  are complex and non-linearly correlated. For these values of  $t$ , we can show that any linear combination of  $\mathbf{k}_1$  and  $\mathbf{k}_2$  will always be complex valued.  $\Phi(t)$  has no real eigenvector corresponding to zero eigenvalue. Then,  $\mathbf{k}^T \Phi(t) \mathbf{k} \neq 0$ ,  $real\{\mathbf{k}^T \Phi(t) \mathbf{k}\} = \mathbf{k}^T real\{\Phi(t)\} \mathbf{k} \neq 0$ , which means  $real\{\Phi(t)\}$  is full rank, there is no zero eigenvalue.

case 3:  $t = t_3$ . When  $t = t_1$  and  $t_2$ , We have:

$$\begin{aligned}\mathbf{k}^T \Phi(t_1) \mathbf{k} &= \mathbf{k}^T \widehat{\mathbf{A}}^H(t_1) \mathbf{U}_N \mathbf{U}_N^H \widehat{\mathbf{A}}(t_1) \mathbf{k} = 0 \\ \mathbf{k}^T \Phi(t_2) \mathbf{k} &= \mathbf{k}^T \widehat{\mathbf{A}}^H(t_2) \mathbf{U}_N \mathbf{U}_N^H \widehat{\mathbf{A}}(t_2) \mathbf{k} = 0\end{aligned}$$

which are equivalent to

$$\mathbf{U}_N^H \widehat{\mathbf{A}}(t_1) \mathbf{k} = 0$$

$$\mathbf{U}_N^H \widehat{\mathbf{A}}(t_2) \mathbf{k} = 0$$

300 For  $t = t_3$ , any linear combination of above equations leads  $\mathbf{U}_N^H \widehat{\mathbf{A}}(t_1) \mathbf{k} + \alpha \mathbf{U}_N^H \widehat{\mathbf{A}}(t_2) \mathbf{k} = \mathbf{U}_N^H \widehat{\mathbf{A}}(t_3) \{ \widehat{\mathbf{A}}^H(\Delta t) + \alpha \widehat{\mathbf{A}}(\Delta t) \} \mathbf{k} = 0$ . Only when  $\alpha$  is equal to 1 or  $-1$ ,  $\widehat{\mathbf{A}}^H(\Delta t) + \alpha \widehat{\mathbf{A}}(\Delta t)$  is a pure real or imaginary matrix.

For  $\alpha = 1$ ,  $\mathbf{U}_N^H \widehat{\mathbf{A}}(t_3) \{ \widehat{\mathbf{A}}^H(\Delta t) + \widehat{\mathbf{A}}(\Delta t) \} \mathbf{k} = 2 \mathbf{U}_N^H \widehat{\mathbf{A}}(t_3) \text{real}\{ \widehat{\mathbf{A}}(\Delta t) \} \mathbf{k} = 2 \mathbf{U}_N^H \widehat{\mathbf{A}}(t_3) \mathbf{k}_3$ .

For  $\alpha = -1$ ,  $\mathbf{U}_N^H \widehat{\mathbf{A}}(t_3) \{ \widehat{\mathbf{A}}^H(\Delta t) - \widehat{\mathbf{A}}(\Delta t) \} \mathbf{k} = 2j \mathbf{U}_N^H \widehat{\mathbf{A}}(t_3) \text{imag}\{ \widehat{\mathbf{A}}(\Delta t) \} \mathbf{k} = 2j \mathbf{U}_N^H \widehat{\mathbf{A}}(t_3) \mathbf{k}_4$ .

305 Therefore,  $\mathbf{k}_3^T \boldsymbol{\Phi}(t_3) \mathbf{k}_3 = \mathbf{k}_4^T \boldsymbol{\Phi}(t_3) \mathbf{k}_4 = 0$  with  $\mathbf{k}_3 = \text{real}\{ \widehat{\mathbf{A}}(\Delta t) \} \mathbf{k}$  and  $\mathbf{k}_4 = \text{imag}\{ \widehat{\mathbf{A}}(\Delta t) \} \mathbf{k}$ .

In addition,  $\mathbf{a}^H(t) \mathbf{U}_N \mathbf{U}_N^H \mathbf{a}(t)$  is always real valued, thus,  $t_3$  is a solution of  $\lambda_{\min}(t) = 0$  and  $\text{real}\{ \boldsymbol{\Phi}(t_3) \}$  only two zero eigenvalues with corresponding eigenvectors  $\mathbf{k}_3$  and

$\mathbf{k}_4$ . When the number of echoes is superior to 2, the number of zero eigenvalues of  $\text{real}\{ \boldsymbol{\Phi}(t) \}$  corresponding to the true time delay is odd. For false time delay, this

310 number is even.

## Appendix C

In this appendix, we present MLE for the roughness parameters estimation. The time delays are estimated ( $\hat{t}_k$  is the  $k$ th estimated time delay) and the noise being a Gaussian white noise with zero mean and variance  $\sigma^2$ . Referring to Eq. (1), the joint probability density function for all observations can be calculated:

$$f(\mathbf{r}, b_k) = \frac{1}{(\pi\sigma^2)^N} \exp\left\{ -\frac{\sum_{i=1}^N |r(f_i) - \sum_{k=1}^K s_k e(f_i) \exp(-j2\pi f_i \hat{t}_k - b_k f_i^2)|^2}{\sigma^2} \right\}$$

In practice, MLE is obtained by maximizing a log-likelihood function  $L(\mathbf{r}, b_k)$  instead of the joint density function  $f(\mathbf{r}, b_k)$  as follows:

$$\begin{aligned} L(\mathbf{r}, b_k) &= \ln f(\mathbf{r}, b_k) \\ &= -\frac{\sum_{i=1}^N |r(f_i) - \sum_{k=1}^K s_k e(f_i) \exp(-j2\pi f_i \hat{t}_k - b_k f_i^2)|^2}{\sigma^2} - N \ln(\pi\sigma^2) \end{aligned}$$

The optimal estimation (for the roughness parameters  $b_k$ ) is obtained by finding the solution of  $\frac{\partial L(\mathbf{r}, b_k)}{\partial b_k} = 0$ .

### Acknowledgment

315 The authors would like to thank the China Scholarship Council (No. 201306150010) and the grant of science and technology planning project of Guangdong (No. 2015A050502011) for funding part of this work. This work may contribute to COST Action TU1208 “Civil Engineering Applications of Ground Penetrating Radar”.

### References

- 320 [1] A.P. Annan, N. Diamanti, J.D. Redman, S.R. Jackson, Ground-penetrating radar for assessing winter roads, *Geophysics* 81 (2016) WA101–WA109.
- [2] A. Benedetto, L. Pajewski, *Civil Engineering Applications of Ground Penetrating Radar*, Springer International Publishing, Switzerland, 2015.
- 325 [3] A.S. Venkatachalam, X. Xu, D. Huston, T. Xia, Development of a new high speed dual-channel impulse ground penetrating radar, *IEEE Journal of Selected Topics in Applied Earth Observations and Remote Sensing* 7 (2014) 753–760.

- [4] D.H. Chen, F. Hong, W. Zhou, P. Ying, Estimating the hotmix asphalt air voids from ground penetrating radar, *NDT & E International* 68 (2014) 120–127.
- [5] H. Liu, M. Sato, In situ measurement of pavement thickness and dielectric permittivity by GPR using an antenna array, *NDT & E International* 64 (2014) 65–71.
- [6] J. Lee, C. Nguyen, T. Scullion, A novel, compact, low-cost, impulse ground-penetrating radar for nondestructive evaluation of pavement, *IEEE Trans. Instrum. Meas.* 53 (December 2004) 1502–1509.
- [7] T. Saarenketo, T. Scullion, Road evaluation with ground penetrating radar, *Journal of applied geophysics* 43 (2000) 119–138.
- [8] S. Lee, E. Millos, R. Greiner, J. Rossiter, A. Venetsanopoulos, On the machine analysis of radar signals for ice profiling, *Signal Processing* 18 (1989) 371–386.
- [9] U. Spagnolini, V. Rampa, Multitarget detection/tracking for monostatic ground penetrating radar: Application to pavement profiling, *IEEE Transactions on Geoscience and Remote Sensing* 37 (1) (January 1999) 383–394.
- [10] I.L. AL-Qadi, S. Lahouar, Measuring layer thickness with GPR—theory to practice, *Construction and building materials* 19 (10) (2005) 763–772.
- [11] S. Lahouar, I. L. Al-Qadi, Automatic detection of multiple pavement layers from GPR data, *NDT & E International* 41 (2) (2008) 69–81.
- [12] C. Le Bastard, V. Baltazart, Y. Wang, J. Saillard, Thin-pavement thickness

estimation using GPR with high-resolution and super resolution methods, *IEEE Transactions on Geoscience and Remote Sensing* 45 (August 2007) 2511–2519.

- [13] N. Pinel, C. Le Bastard, V. Baltazart, C. Bourlier, Y. Wang, Influence of layer roughness for road survey by ground penetrating radar at nadir: theoretical study, *IET Radar, Sonar & Navigation* 5 (July 2011) 650–656.
- [14] K. Luo, A. Manikas, Superresolution multitarget parameter estimation in MIMO radar, *IEEE Transactions on Geoscience and Remote Sensing* 51 (6) (2013) 3683–3693.
- [15] D. Kurrant, E. Fear, Technique to decompose near-field reflection data generated from an object consisting of thin dielectric layers, *IEEE Transactions on Antennas and Propagation* 60 (8) (2012) 3684–3692.
- [16] C. Le Bastard, V. Baltazart, Y. Wang, Modified ESPRIT (M-ESPRIT) algorithm for time delay estimation in both any noise and any radar pulse context by a GPR radar, *Signal Processing* 90 (2010) 173–179.
- [17] K. Chahine, V. Baltazart, Y. Wang, Interpolation-based matrix pencil method for parameter estimation of dispersive media in civil engineering, *Signal Processing* 90 (2010) 2567–2580.
- [18] N. Pinel, C. Le Bastard, C. Bourlier, M. Sun, Asymptotic Modeling of Coherent Scattering from Random Rough Layers: Application to Road Survey by GPR at Nadir, *Int. Journal of Antennas and Propagation* (2012) Article ID 874840.
- [19] M. Sun, N. Pinel, C. Le Bastard, V. Baltazart, A. Ihamouten, Y. Wang, Time

delay and interface roughness estimation by subspace algorithms for pavement survey by radar, *Near Surface Geophysics* 13 (June 2015) 279–287.

- 370 [20] M. Sun, C. Le Bastard, N. Pinel, Y. Wang, J. Li, Road surface layers geometric parameters estimation by ground penetrating radar using Estimation of Signal Parameters via Rotational Invariance Techniques method, *IET Radar, Sonar & Navigation* 10 (2016) 603–609.
- [21] L. Qu, Q. Sun, T. Yang, L. Zhang, Y. Sun, Time-delay estimation for ground penetrating radar using ESPRIT with improved spatial smoothing preprocessing, *IEEE Geoscience and remote sensing letters* 11 (2014) 1315–1319.
- 375 [22] A. Schatzberg, A. J. Devaney, A. J. Witten, Estimating target location from scattered field data, *Signal Processing* 40 (1994) 227–237.
- [23] N. Déchamps, N. de Beaucoudrey, C. Bourlier, S. Toutain, Fast numerical method for electromagnetic scattering by rough layered interfaces: Propagation-inside-layer expansion method, *J. Opt. Soc. Am. A.* 23 (2006) 359–369.
- 380 [24] C. Bourlier, G. Kubické, N. Déchamps, Fast method to compute scattering by a buried object under a randomly rough surface: PILE combined with FB-SA, *J. Opt. Soc. Am. A.* 5 (2009) 260–263.
- [25] C. Bourlier, C. Le Bastard, V. Baltazart, Generalization of PILE method to the EM scattering from stratified subsurface with rough interlayers: application to the detection of debondings within pavement structure, *IEEE Transactions on Geoscience and Remote Sensing* 53 (2015) 4104–4115.
- 385

- [26] F. Koudogbo, P. F. Combes, H. J. Mametsa, Numerical and experimental  
390 validations of IEM for bistatic scattering from natural and manmade rough  
surfaces, *Progress In Electromagnetics Research* 46 (2004) 203–244.
- [27] E. Li, K. Sarabandi, Low grazing incidence millimeter-wave scattering models  
and measurements for various road surfaces, *IEEE Transactions on Antennas  
and Propagation* 47 (1999) 851–861.
- 395 [28] C. Fauchard, Utilisation de radars très hautes fréquences: application à lauscul-  
tation non destructive des chaussées, PhD thesis, University of Nantes, France,  
2001.
- [29] D. Daniel, *Ground Penetrating Radar*, IEE Press, London, 2nd edn, 2004.
- [30] X. Li, R. Wu, an efficient algorithm for time delay estimation, *IEEE Transac-  
400 tions on Signal Processing* 46 (1998) 2231–2235.
- [31] M. Sun, C. Le Bastard, Y. Wang, N. Pinel, Time delay estimation using ESPRIT  
with extended improved spatial smoothing techniques for radar signals, *IEEE  
Geoscience and Remote Sensing Letters* 13 (2016) 73–77.
- [32] B. Friedlander, A. J. Weiss, Direction finding using spatial smoothing with  
405 interpolated arrays, *IEEE Transactions on Aerospace and Electronic Systems*  
28 (1982) 574–587.
- [33] A. J. Weiss, B. Friedlander, performance analysis of spatial smoothing with  
interpolated arrays, *IEEE Transactions on Signal Processing* 41 (1993) 1881–  
1892.

- 410 [34] S. Marcos, J. Sanchez-Araujo, Méthodes linéaires haute résolution pour  
l'estimation de directions d'arrivée de sources. Performances asymptotiques et  
complexité, *Traitement du Signal* 14 (1997) 99–116.
- [35] T. J. Shan, M. Wax, T. Kailath, On spatial smoothing for direction-of-arrival  
estimation of coherent signals, *IEEE Transactions on Acoustics, Speech and*  
415 *Signal Processing* 33 (1985) 806–811.
- [36] F. Ge, D. Shen, Y. Peng, V.O.K. Li, Super-Resolution Time Delay Estimation  
in Multipath Environments, *IEEE Transactions on Circuits and Systems* 54  
(2007) 1977–1986.
- [37] F. Ge , Q. Wan , X. Wang, Y. Peng, Frequency estimation of the sinusoidal  
420 signals with lowpass envelopes based on the eigenanalysis, in *IEEE Radar Conf.*  
(2002) 453–458.

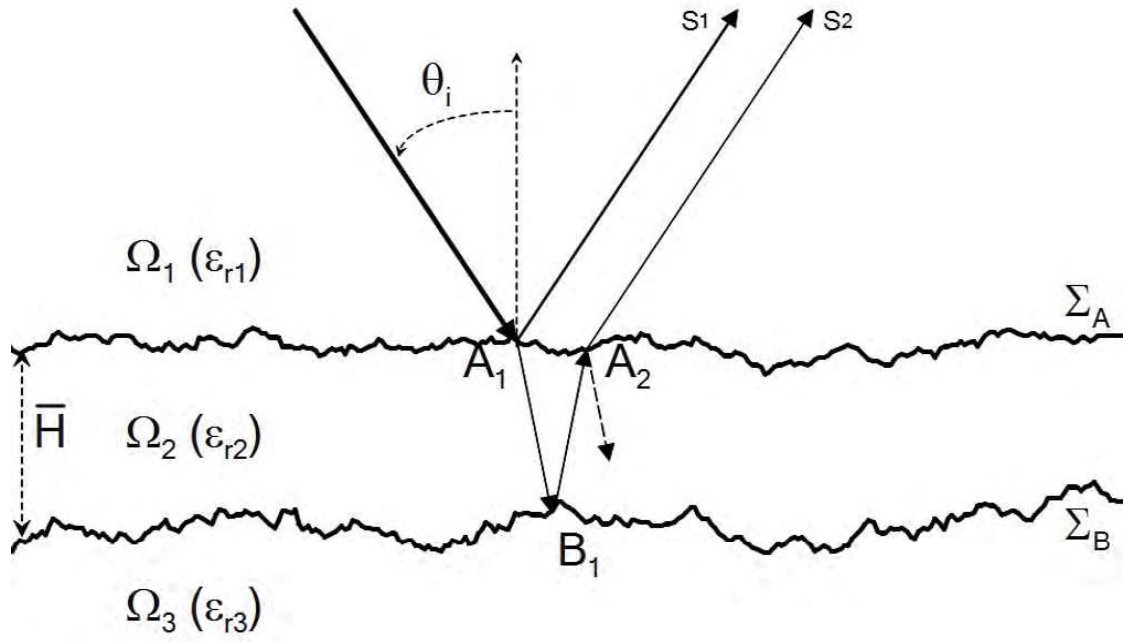


Figure 1: Rough Pavement Configuration.

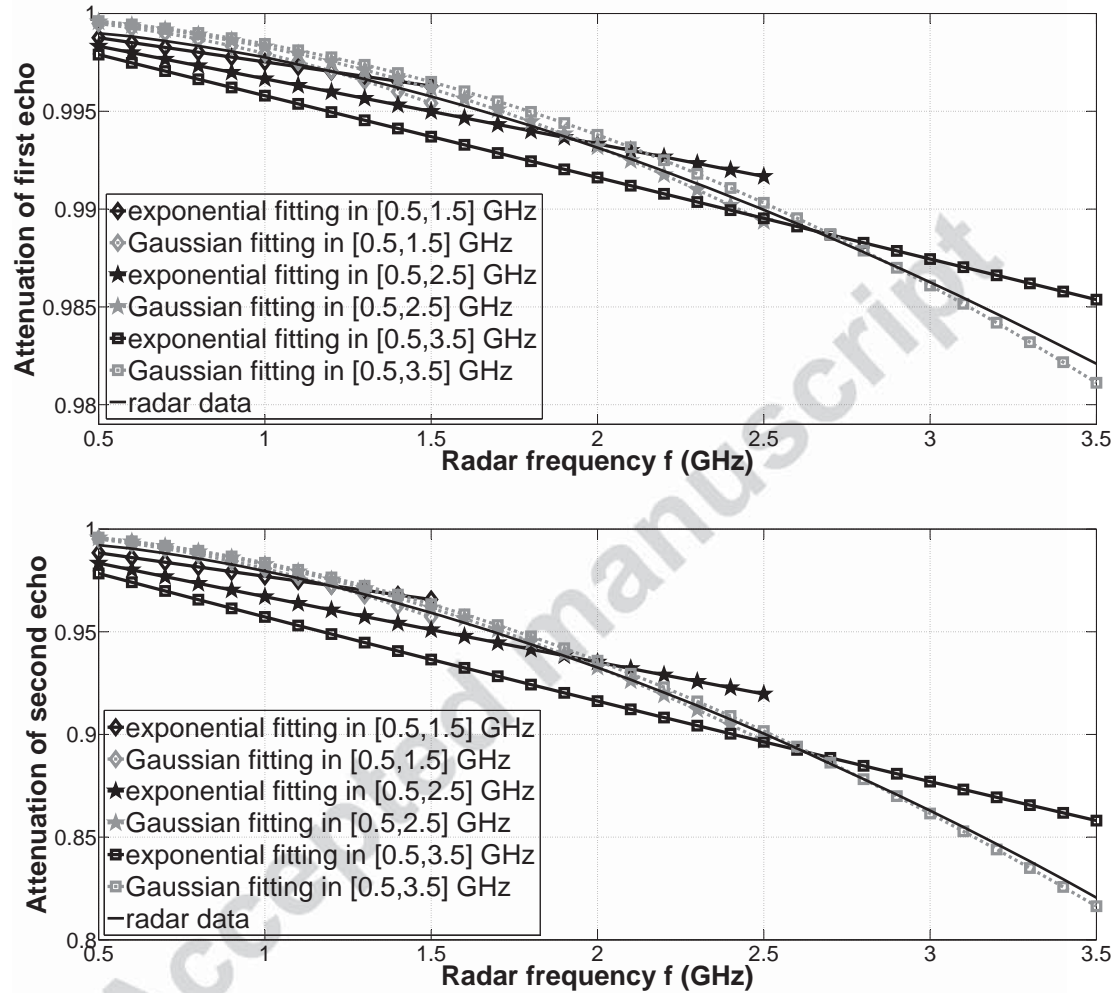


Figure 2: Frequency behaviour of echoes with curve fitting results in [0.5, 1.5] GHz, [0.5, 2.5] GHz and [0.5, 3.5] GHz.

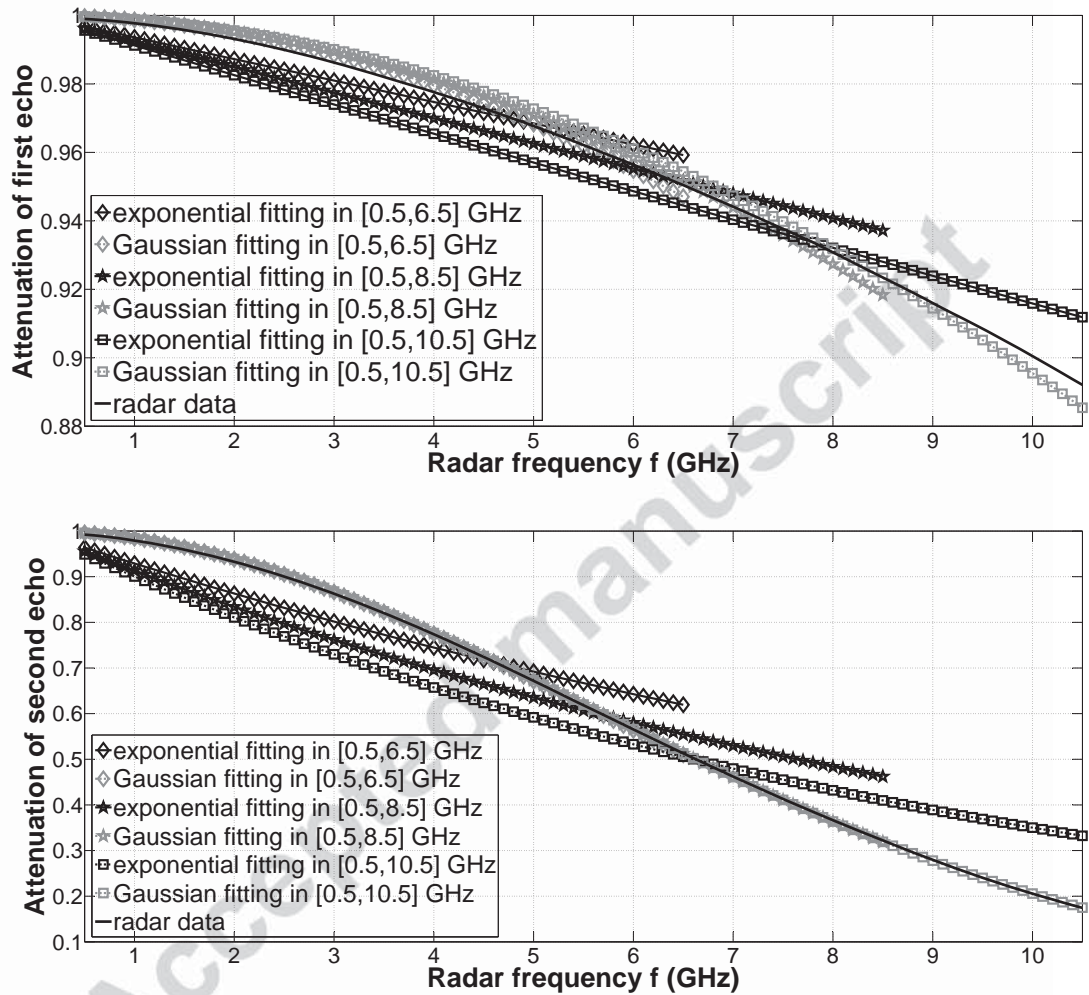


Figure 3: Frequency behaviour of echoes with curve fitting results in [0.5, 6.5] GHz, [0.5, 8.5] GHz and [0.5, 10.5] GHz.

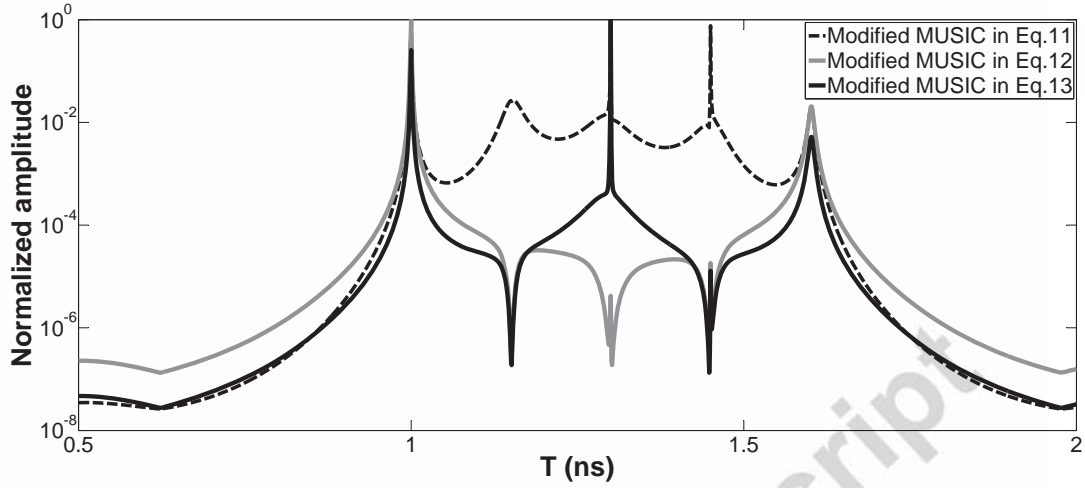


Figure 4: Pseudo-spectrum of MUSIC for time delay estimation with SNR=30 dB, the three time delays are 1 ns, 1.3 ns and 1.6 ns.

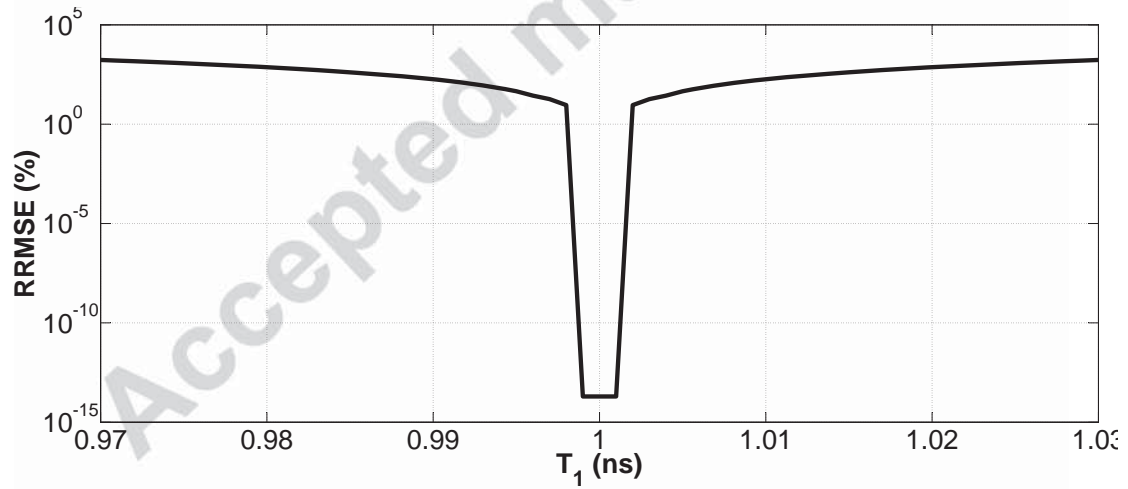


Figure 5: RRMSE on the estimated roughness parameter  $b_1 = 1.10 \times 10^{-3} \text{ GHz}^{-2}$  ( $\sigma_{hA} = 0.5 \text{ mm}$ ,  $L_{cA} = 6.4 \text{ mm}$ ) against first time delay  $T_1 = 1 \text{ ns}$  in a noiseless environment by MLE.

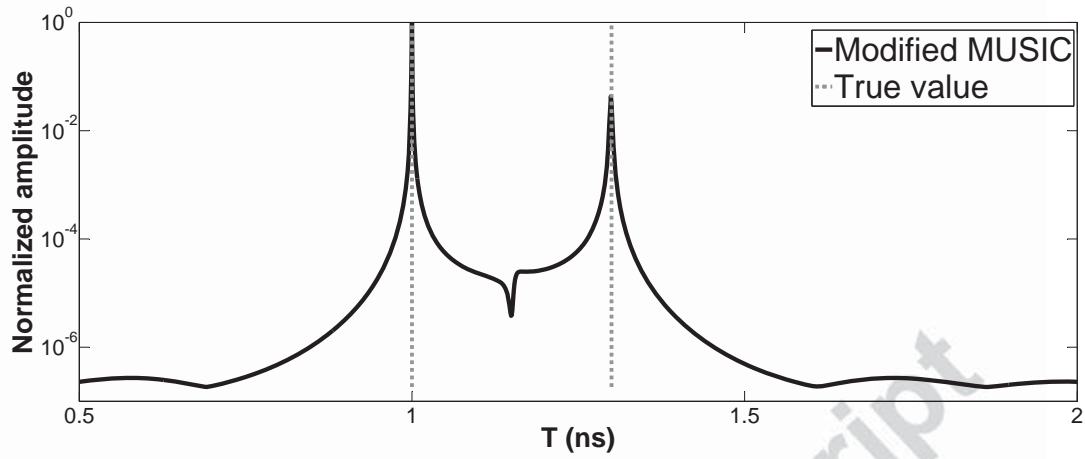


Figure 6: Case 1, Pseudo-spectrum of MUSIC for time delay estimation with SNR=20 dB, the two time delays are 1 ns and 1.3 ns in grey dashed line, slightly overlapped.

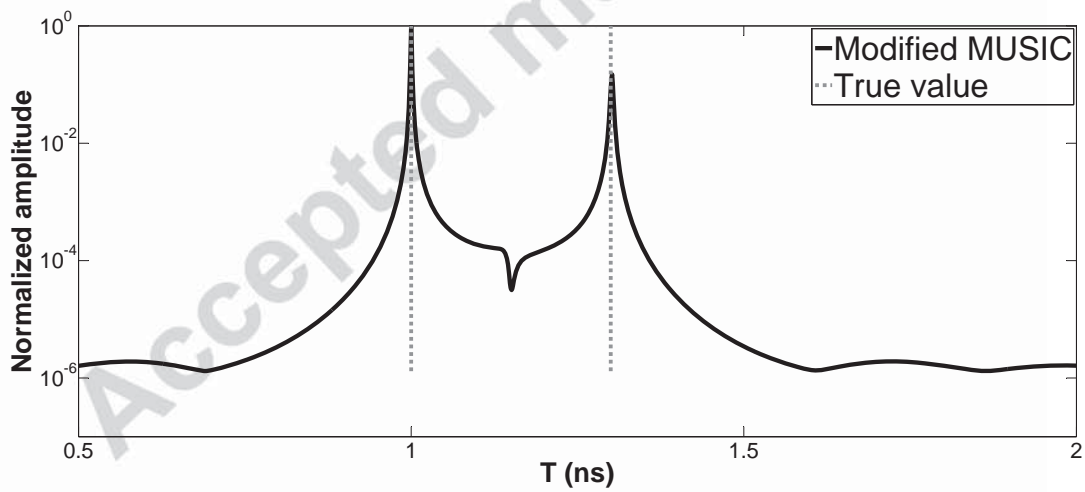


Figure 7: Case 2, Pseudo-spectrum of MUSIC for time delay estimation with SNR=20 dB, the two time delays are 1 ns and 1.3 ns in grey dashed line, slightly overlapped.

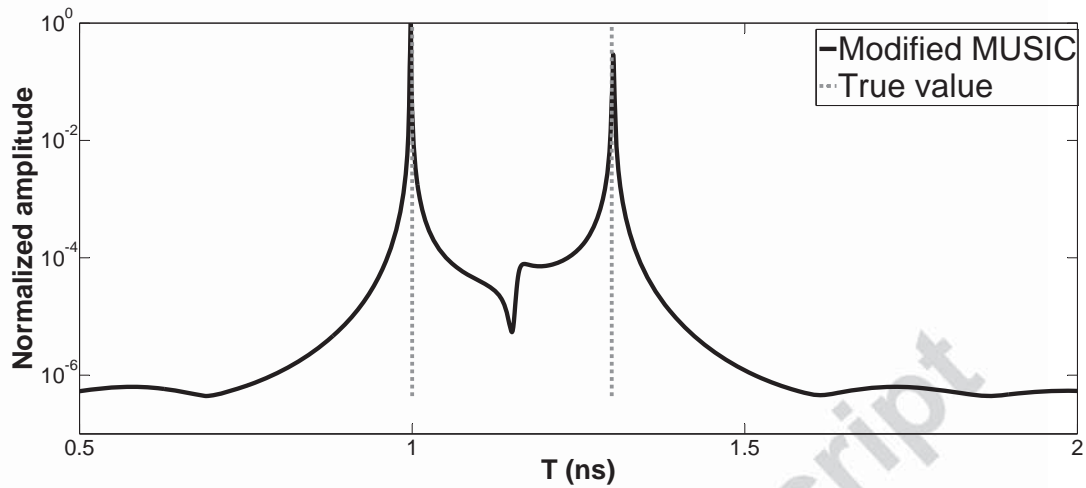


Figure 8: Case 3, Pseudo-spectrum of MUSIC for time delay estimation with SNR=20 dB, the two time delays are 1 ns and 1.3 ns in grey dashed line, slightly overlapped.

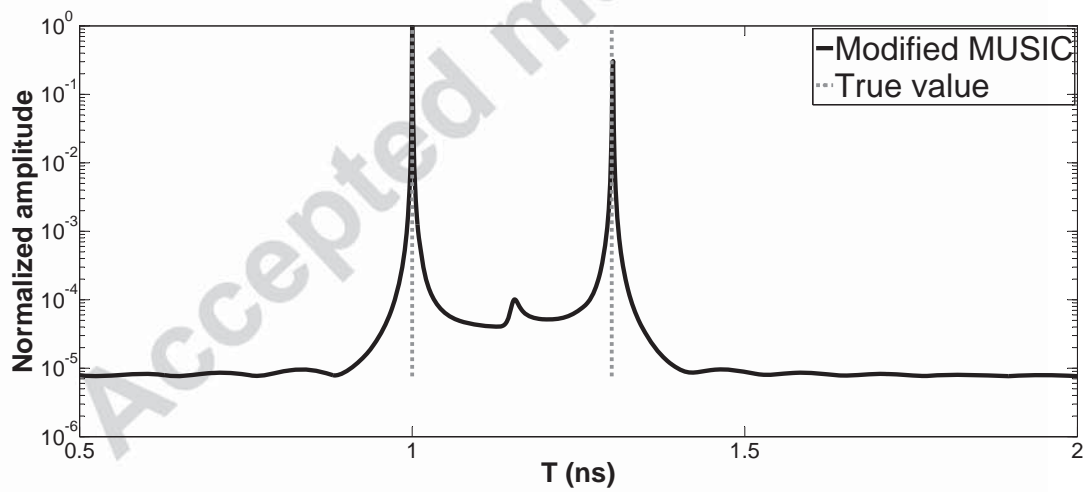


Figure 9: Case 1, Pseudo-spectrum of MUSIC for time delay estimation with SNR=20 dB, the two time delays are 1 ns and 1.3 ns in grey dashed line, non-overlapped.

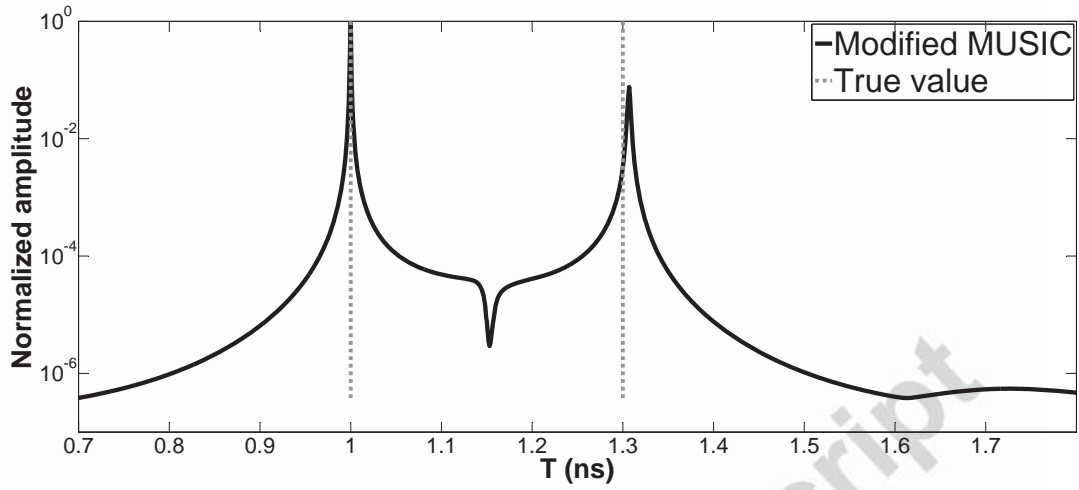


Figure 10: Case 4, Pseudo-spectrum of MUSIC for time delay estimation with SNR=20 dB, the two time delays are 1 ns and 1.3 ns in grey dashed line, slightly overlapped, low-loss media.

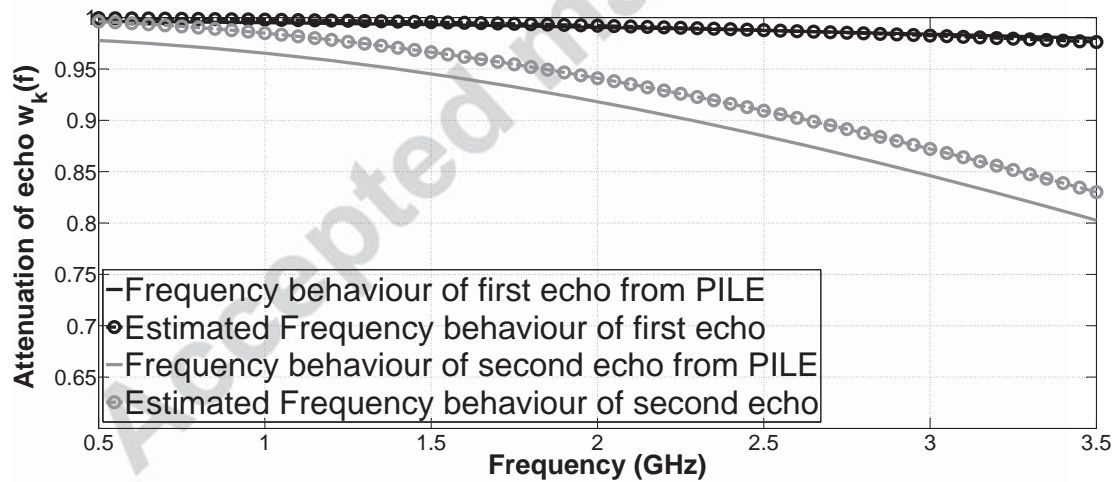


Figure 11: Case 1, Expression for frequency behaviour of backscattered echoes by using estimated roughness parameter versus frequency behaviour of backscattered echoes from radar data, slightly overlapped.

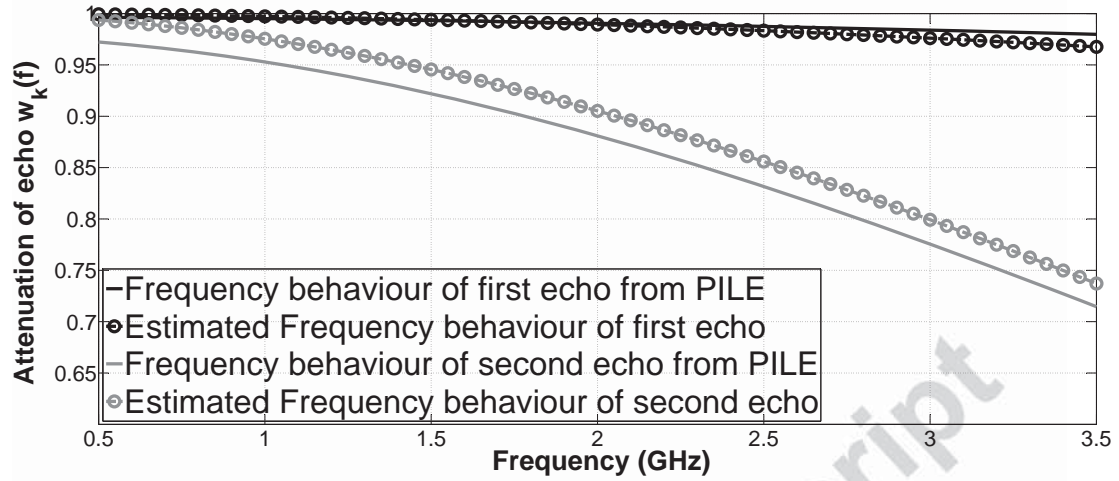


Figure 12: Case 2, Expression for frequency behaviour of backscattered echoes by using estimated roughness parameter versus frequency behaviour of backscattered echoes from radar data, slightly overlapped.

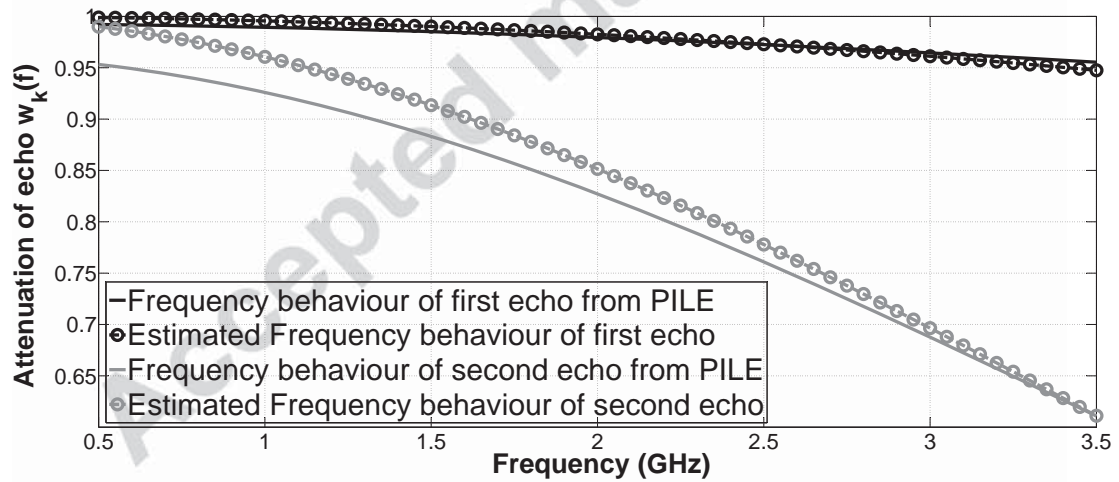


Figure 13: Case 3, Expression for frequency behaviour of backscattered echoes by using estimated roughness parameter versus frequency behaviour of backscattered echoes from radar data, slightly overlapped.

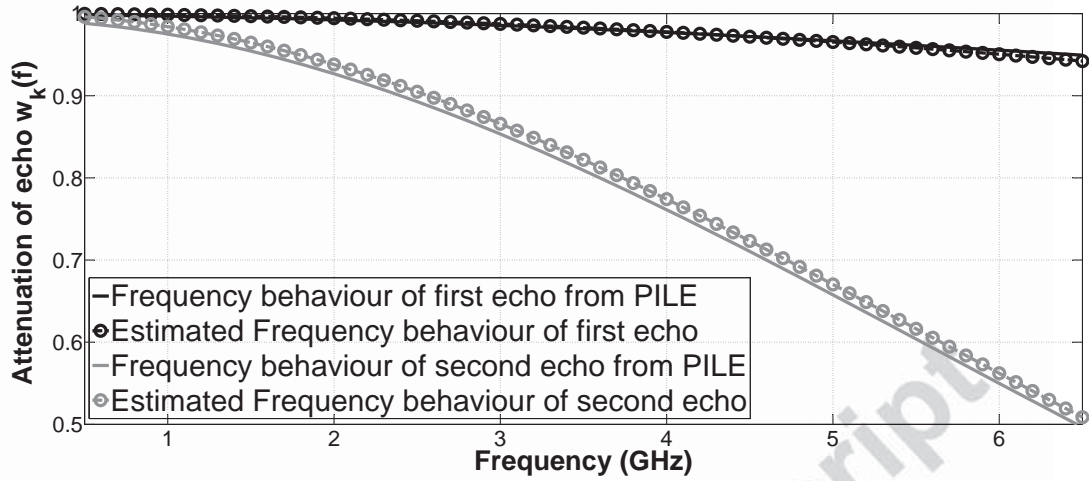


Figure 14: Case 1, Expression for frequency behaviour of backscattered echoes by using estimated roughness parameter versus frequency behaviour of backscattered echoes from radar data, non-overlapped.

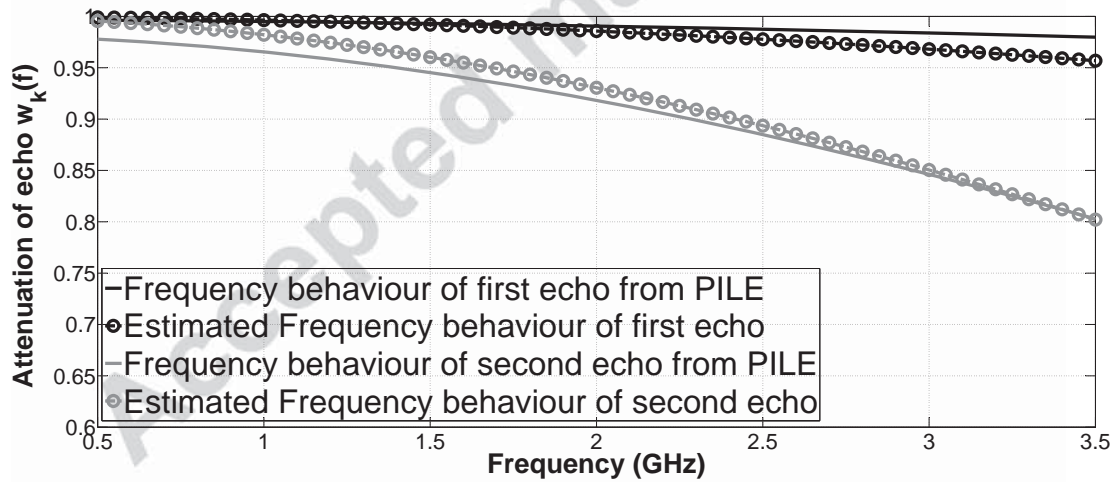


Figure 15: Case 4, Expression for frequency behaviour of backscattered echoes by using estimated roughness parameter versus frequency behaviour of backscattered echoes from radar data, slightly overlapped, low-loss media.

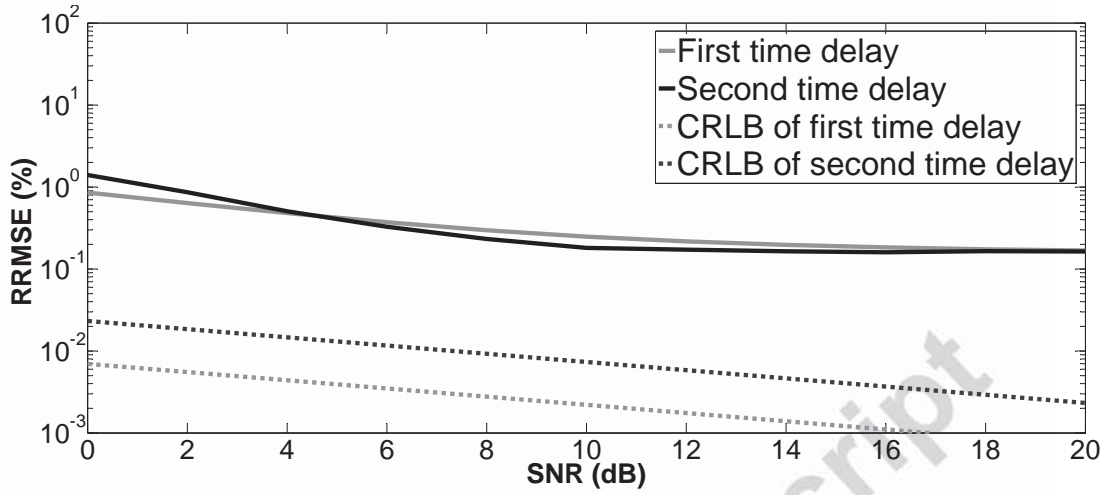


Figure 16: Simulation 2, RRMSE on the estimated time delay  $t_k$ , ( $k = 1, 2$ ) vs. SNR after 500 Monte-Carlo simulations for case 1, slightly overlapped.

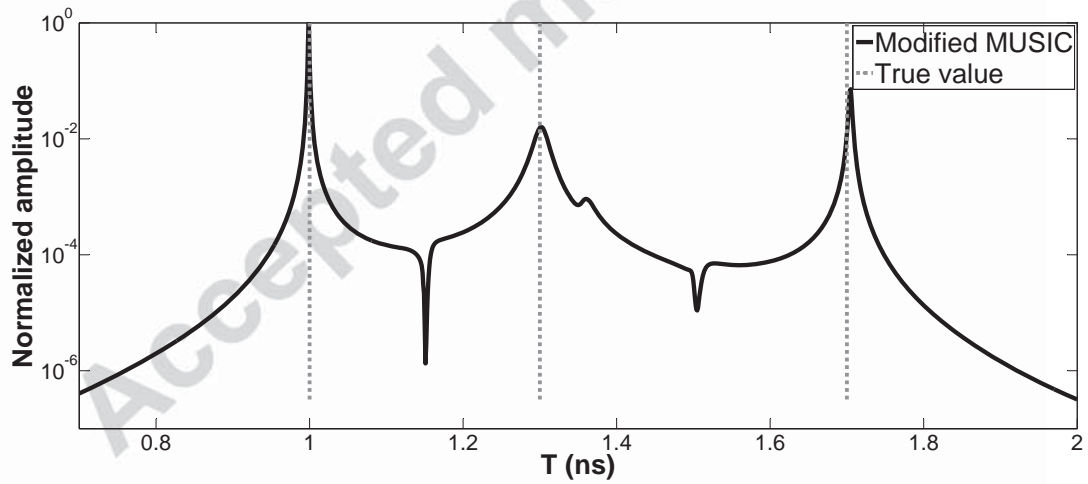


Figure 17: Simulation 3, Pseudo-spectrum of MUSIC for time delay estimation with SNR=20 dB, the three time delays are 1 ns, 1.3 ns and 1.7 ns in grey dashed line.

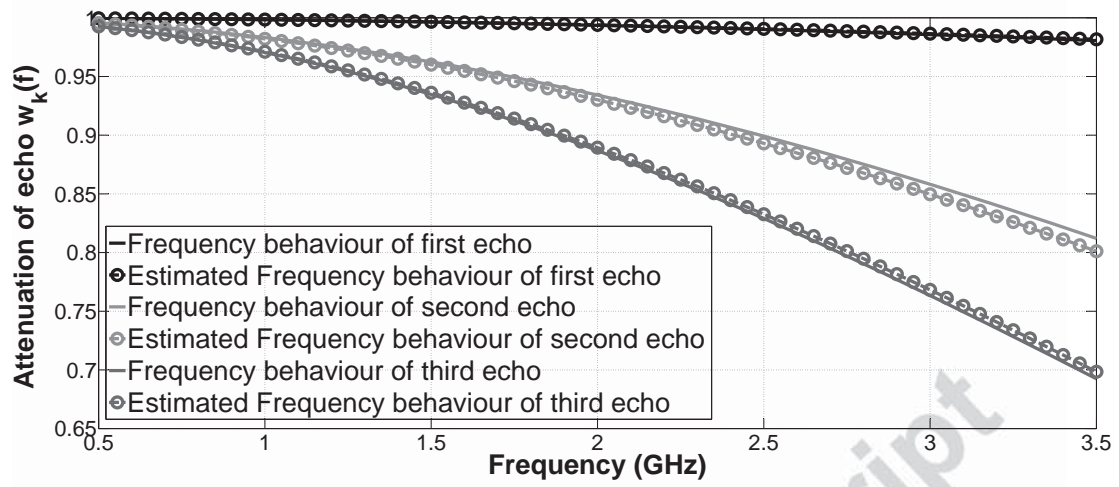


Figure 18: Simulation 3, Expression for frequency behaviour of backscattered echoes by using estimated roughness parameter versus frequency behaviour of backscattered echoes from radar data.

RMSE $\% (s_1/s_2)$ \ Frequency	Model	$ s(f)  = s_k \times \exp(-\bar{b}f)$	$ s(f)  = s_k \times \exp(-bf^2)$
[0.5, 1.5] <i>GHz</i>		0.0290/0.371	0.0307/0.179
[0.5, 2.5] <i>GHz</i>		0.0906/1.04	0.0433/0.257
[0.5, 3.5] <i>GHz</i>		0.171/1.94	0.0605/0.324
[0.5, 6.5] <i>GHz</i>		0.463/5.63	0.170/0.346
[0.5, 8.5] <i>GHz</i>		0.698/7.99	0.270/0.355
[0.5, 10.5] <i>GHz</i>		0.983/9.88	0.367/0.323

Table 1: RMSE on curve fitting with Gaussian and exponential functions.

Parameter	case1 overlapped	case2 overlapped	case3 overlapped	case1 non-overlapped	case1 overlapped with low-loss media
$\hat{t}_1$ (ns)	1.000	1.000	0.999	1.000	1.000
$\hat{t}_2$ (ns)	1.299	1.302	1.301	1.302	1.306
$\hat{b}_1$ (GHz <sup>-2</sup> )	$1.96 \times 10^{-3}$	$2.69 \times 10^{-3}$	$4.40 \times 10^{-3}$	$1.41 \times 10^{-3}$	$3.52 \times 10^{-3}$
$\hat{b}_2$ (GHz <sup>-2</sup> )	$1.52 \times 10^{-2}$	$2.49 \times 10^{-2}$	$4.02 \times 10^{-2}$	$1.60 \times 10^{-2}$	$1.76 \times 10^{-2}$

Table 2: Estimated time delays and roughness parameters by modified MUSIC and MLE.  $\hat{t}_k$  and  $\hat{b}_k$  represent estimated time delays and estimated roughness parameters, respectively.